# Prediction of human errors by maladaptive changes in event-related brain networks

Tom Eichele*†, Stefan Debener‡, Vince D. Calhoun§¶‖, Karsten Specht*,**, Andreas K. Engel††, Kenneth Hugdahl*,**, D. Yves von Cramon‡‡, and Markus Ullsperger‡‡§§

*Department of Biological and Medical Psychology, University of Bergen, 5009 Bergen, Norway; ‡Medical Research Council Institute of Hearing Research, Southampton SO14 OYG, United Kingdom; §MIND Institute, Albuquerque, NM 87131; ¶Department of Electrical and Computer Engineering, University of New Mexico, Albuquerque, NM 87131; ‖Department of Psychiatry, Yale University School of Medicine, New Haven, CT 06520; **Haukeland University Hospital, 5021 Bergen, Norway; ††Department of Neurophysiology and Pathophysiology, University Medical Center Hamburg–Eppendorf, 20246 Hamburg, Germany; ‡‡Max Planck Institute for Human Cognitive and Brain Sciences, 04103 Leipzig, Germany; and §§Max Planck Institute for Neurological Research, 50931 Cologne, Germany

Edited by Marcus E. Raichle, Washington University School of Medicine, St. Louis, MO, and approved March 4, 2008 (received for review September 21, 2007)

**Humans engaged in monotonous tasks are susceptible to occasional errors that may lead to serious consequences, but little is known about brain activity patterns preceding errors. Using functional MRI and applying independent component analysis followed by deconvolution of hemodynamic responses, we studied error preceding brain activity on a trial-by-trial basis. We found a set of brain regions in which the temporal evolution of activation predicted performance errors. These maladaptive brain activity changes started to evolve ≈30 sec before the error. In particular, a coincident decrease of deactivation in default mode regions of the brain, together with a decline of activation in regions associated with maintaining task effort, raised the probability of future errors. Our findings provide insights into the brain network dynamics preceding human performance errors and suggest that monitoring of the identified precursor states may help in avoiding human errors in critical real-world situations.**

deconvolution | performance monitoring | default mode | frontal lobe

Human behavior may be strongly determined by the ongoing intrinsic dynamics of regional brain networks (1–3). Although it is conceivable that patterns of brain activity preceding action execution are causally responsible for the behavioral outcome, previous research of human performance monitoring typically focused on brain activity evoked by and occurring after behavioral errors and the ensuing adaptive compensatory mechanisms (4–6). It is not known yet how far ahead in time the state of cortical brain networks impacts on behavioral performance; some EEG and functional MRI (fMRI) evidence exists suggesting that activity in the preceding trial foreshadows subsequent errors but not earlier than that (7–10). The present study investigated this question by means of a single-trial analysis of event-related independent components (IC) in fMRI data during a visual task requiring rapid responses.

We analyzed patterns of evoked brain activity across trials that preceded erroneous behavior and may thus be instrumental in causing errors. Errors in this simple repetitive forced-choice task in a controlled setting may principally have two mutually nonexclusive causes: One source of errors consists simply of random failures to implement the correct behavior, which may be generated by momentary fluctuations in neural activity during stimulus processing and response selection in a given trial (1, 11). Although it is possible to make predictions about adaptive behavior in trials succeeding an error, it would be largely impossible in this condition to anticipate future errors from current brain states. Another possibility is that a proportion of errors may be caused by a systematic maladjustment in cognitive control systems that develops more slowly over time, and which thus affords a prediction about future behavior, in particular the likelihood of an erroneous response from analyzing trends in the history of activity across trials.

Models of cognitive control propose a performance-monitoring system involving the posterior medial frontal cortex (pMFC). This system tracks unfavorable outcomes and signals the need for appropriate behavioral adjustments (4, 6), which are thought to be initiated by enhancing and updating context and rule representations, thereby optimizing goal-directed behavior (12, 13). Notably, this performance-monitoring system signals the need for adjustment, which is required in response after errors and feedback and, more generally, whenever action outcome is at risk, for example, during response conflict (4). Maladjustment within cognitive control processes could build up gradually over a longer period and may be expressed as a decline of task-related attention and effort (14) and/or failure to suppress neural activity that interferes with performance.

An important source of activity that may interfere with behavioral performance is the so-called default mode network (DMN), a set of regions in the brain encompassing the precuneus, retrosplenial cortex, and anterior medial frontal cortex, which show increased metabolism during passive resting conditions (15, 16). These regions show correlated spontaneous fluctuations of hemodynamic activity among each other during relaxed wakefulness (17), that persist in sleep (18) and sedation (19). Also, anticorrelations between the DMN and regions relevant in diverse cognitive operations have been observed with functional connectivity analysis of fMRI data (2, 20, 21). The DMN is consistently extracted with other data-driven analysis techniques such as independent component analysis (ICA) of fMRI data recorded during relaxed resting (22), discrete sensory stimulation (23), continuous natural stimulation (24), and task performance (25). Additionally, the DMN has been linked to features in resting-state (26, 27) and event-related EEG (28). The range of functions that might involve the DMN and its interaction with other networks remains to be explored (29–31). For our inquiry, it is important that, whereas DMN activity is typically suspended in the presence of cognitive tasks, parts of it are less deactivated to commission errors (10), and similarly reduced deactivation is found in stimulus-evoked hemodynamic

Author contributions: S.D., A.K.E., D.Y.v.C., and M.U. designed research; S.D. and M.U. performed research; T.E. and V.D.C. contributed new reagents/analytic tools; T.E., S.D., V.D.C., K.S., and M.U. analyzed data; and T.E., S.D., V.D.C., K.S., A.K.E., K.H., D.Y.v.C., and M.U. wrote the paper.

The authors declare no conflict of interest.

This article is a PNAS Direct Submission.

Freely available online through the PNAS open access option.

Data deposition: The fMRI dataset has been deposited in the Mind Research database, http://portal.mind.unm.edu/dcon/.

†To whom correspondence should be addressed. E-mail: tom.eichele@psybp.uib.no.

This article contains supporting information online at www.pnas.org/cgi/content/full/0708965105/DCSupplemental.

responses during momentary lapses of attention, as defined by a slow response-time criterion in a visual attention task (11). Reduced activation in anterior cingulate and right prefrontal regions during the immediate prestimulus period has been associated with subsequent lapses (11), suggesting an antagonistic relationship between the DMN and areas controlling attention that is relevant for the outcome of goal-directed behavior.

Although Weissman *et al.* (11) focused primarily on the correlation between reaction time and activity patterns, the current analysis explores whether activity patterns that precede overt behavior foreshadow the outcome accuracy in some systematic way. We therefore assessed the relationship between errors in behavioral performance and the amplitude modulation of hemodynamic responses in error-preceding trials. In particular, we addressed the question how far ahead in time the state of brain networks impacts on behavioral accuracy. Such an analysis can provide important knowledge about the functionality of performance monitoring and causes of behavioral errors based on activity trends before the response and also yields measures that may aid in monitoring the likelihood of errors in real-world situations before a response is made.

In the flanker task we used [supporting information (SI) Fig. S1], errors are usually based on premature responses issued before stimulus analysis is completed (32). On incompatible trials, response conflict arises because the salient but distracting flankers and the target arrow drive two competing response tendencies. Errors occur if the flanker-induced response tendency is executed while the target-induced response tendency is still evolving (13). Performing correctly on trials involving high response conflict is cognitively demanding and engages a broad task-related network of brain regions, in particular the pMFC and lateral frontal, premotor, and anterior insular cortices and the intraparietal sulcus (12, 33, 34). Although functionally separable, these regions are overlapping with the proposed dorsal top-down attentional system (35), which has been reported to be anticorrelated to the DMN (21).

Here, we report on a set of brain regions in which activation patterns anticipate the accuracy of behavioral performance at least 6 sec ahead in time. To extract error-preceding activity, we analyzed data from participants who performed a speeded visual flanker task while blood oxygenation level-dependent response (BOLD) fMRI data were collected. In this task, participants had to respond to briefly presented arrows as quickly as possible. Trials consisted of either response-compatible or -incompatible flanker arrows inducing low- and high-response conflict, respectively. Performance errors and timing feedback resulted in behavioral adjustments such as speed/accuracy tradeoff. We have previously demonstrated the role of the pMFC in monitoring errors and influencing subsequent response time adjustments using an EEG-informed fMRI analysis of these data (36). Here, we focus on the identification of fMRI signals that systematically predict errors. This is challenging, because it is usually not possible to specify a model regarding the actual timing and modulation of the underlying precursor signals and adequate parameters of the associated hemodynamic response function (HRF). Therefore, we used a data-driven approach and decomposed the fMRI data with spatial ICA (37, 38). After ICA, we deconvolved HRFs from the timecourses of individual event-related components (ICs) to recover individually and regionally specific empirical estimates of the HRF (39, 40) and used these subsequently for estimation of single-trial responses. Thereby, we effectively removed the effect of hemodynamic convolution and recovered the trial-by-trial amplitude modulation of event-related responses (Fig. 2). With this analysis, four ICs were identified that reliably reflected brain activity modulated by task conditions and that collectively predicted errors (Fig. 1 and Table S1). In this set of brain regions, the temporal evolution of hemodynamic activation-predicted performance errors at least 6 sec ahead in time, with linear trends starting as early as 30 sec before an erroneous response. A coincident decrease of deactivation in regions of the DMN, together with a decline of activation in frontal regions associated with resource allocation and maintaining task effort, raised the probability of future errors.

## Results

**Behavioral Data.** Participants made errors on 0.58% (SEM 0.16) of compatible and 17.23% (SEM 2.17) of incompatible trials (significant difference; $t_{12}$ 7.75; $P < 0.001$). Hit reaction times were 380.8 ms (SEM 7.9) for compatible and 445.0 ms (SEM 8.1) for incompatible trials (significant difference; $t_{12}$ 21.26; $P < 0.001$). The individually adjusted response deadline (mean, 475.7 ms; SEM 17.7) was missed in 9.46% (SEM 1.8) of compatible and in 27.69% (SEM 3.50) of incompatible trials. Error reaction times for incompatible trials (308.2 ms; SEM 9.8) were significantly shorter than for incompatible correct trials ($t_{12} = 4.41$; $P < 0.001$). An illustration of the response-time distributions for compatible, incompatible, error, and feedback trials is provided in Fig. S2. Sequences around error and feedback trials are shown in Fig. S3.

**fMRI Data.** IC 1 represented a pattern of activation in the pMFC encompassing the rostral cingulate zone and presupplementary motor area (pre-SMA), with additional activation in the dorsal premotor cortex, the right inferior frontal junction, and the anterior insula (Ins) bilaterally (Fig. 1*a*). These regions are commonly observed in performance monitoring, including response conflict, errors, feedback, and subsequent adjustments (4). The associated HRF (Fig. 1*b*) displayed a positive peak at 4 sec poststimulus, followed by an undershoot at 9 sec and a subsequent return to baseline. Importantly, IC 1 was differentially activated in task processing ($F_{5,60}$ 6.18; $P < 0.001$) and showed the largest raw data amplitudes to feedback ($t_{12}$ 11.42; $P < 0.001$) and error trials ($t_{12}$ 9.89; $P < 0.001$), consistent with its role in performance monitoring. When the variability associated with the main effects of this component was removed, no significant amplitude modulation preceding or succeeding error trials remained.

IC 2 encompassed left-dominant sensorimotor activity in pre/postcentral gyri and SMA (Fig. 1*d*), which is consistent with the finding that bimanual motor tasks show stronger involvement of the dominant hemisphere in right-handed individuals (41). The HRF had a peak latency at 4 sec without discernible undershoot (Fig. 1*e*). Strongest activation was seen in response to fast incompatible correct responses ($t_{12}$ 12.20; $P < 0.001$), together with an overall difference between the means ($F_{5,60}$ 4.16, $P = 0.003$). Interestingly, activity in IC 2 approached a significant reduction in the immediate error-preceding trial $T_{-1}$ ($t_{12} = -2.07$, $P = 0.06$) (Fig. 1*f*).

IC 3 was composed of two regions, the orbital part of the right inferior frontal gyrus, posterior orbital gyrus (orbitofrontal cortex, OFC), extending into the adjacent inferior anterior insula, and the superior pMFC (pre-SMA, BA 8m) (Fig. 1*g*). The associated HRF peaked at 6 sec and displayed a sustained undershoot from 9 to 16 sec (Fig. 1*h*). The component shows a significant, although weaker, difference between the condition means ($F_{5,60}$ 2.40, $P = 0.05$) and, as in IC 2, the largest activation was seen to fast incompatible correct responses ($t_{12}$ 9.46; $P < 0.001$). Before errors, the activity of IC 3 at $T_{-1}$ was significantly reduced ($t_{12} = -2.64$, $P = 0.02$) and linearly decreased from $T_{-6}$ through $T_{-1}$ ($t_{12} = -2.37$, $P = 0.04$) (Fig. 1*i*). Similar brain areas have been found activated previously during the flanker task (33, 34) and under conditions of increased motivation and effort in a memory task (42). IC 3 shows remarkable overlap with the network suggested to underlie "stable maintenance of task mode

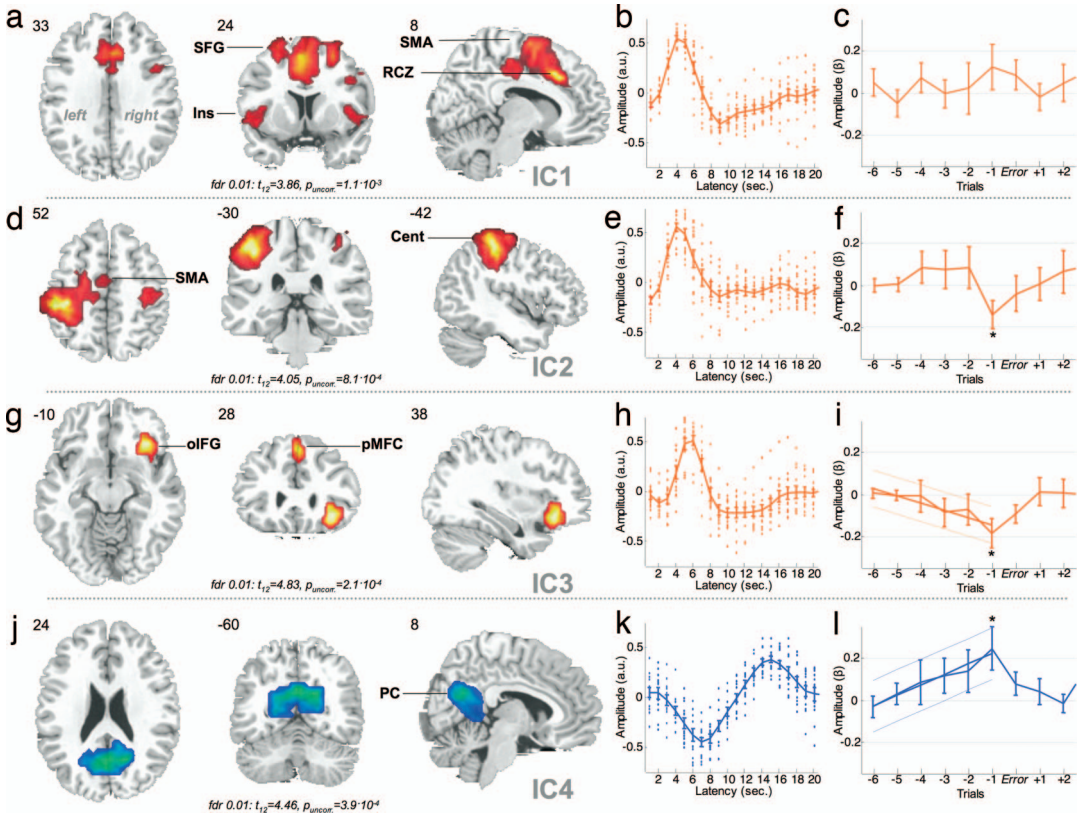


**Fig. 1.** Component maps, hemodynamic responses, and functional modulation. *a*, *d*, *g*, and *j* show the activation maps of the four ICs rendered onto the MNI template at representative transverse (*Left*), coronal (*Center*), and sagittal (*Right*) slices, coordinates in millimeters are given at the top-right corners. The maps are shown in neurological convention (left hemisphere is on the left). IC areas were considered significant when exceeding a cluster extent of at least 27 contiguous voxels, and at 1% false-positive discovery rate, thresholds are given below each IC map. Activations are plotted in red, deactivations in blue. *b*, *c*, *e*, *f*, *h*, *i*, *k*, and *l* display the HRFs within the respective ICs as estimated via deconvolution from 1 to 20 sec after stimulus onset, in arbitrary units. The group average from the 13 participants is plotted as a solid line; error bars indicate ± 1 SEM, and dots represent all individual estimates. The empirical HRFs were used to estimate single-trial amplitudes in the fMRI data to assess systematic preerror activity, here group averaged (±1 SEM) trial sequences from −6 to +2 around response errors are shown (*c*, *f*, *i*, and *l*). These plots represent the residual data after removal of variability accounted for by response conflict, feedback, stimulus sequence, and response times.

and strategy" found in a functional connectivity analysis (43). Based on animal studies, it has been suggested that both the OFC and pMFC code the cost and benefit of actions in terms of reward delay (OFC) and effort (pMFC) (6, 44, 45). Accordingly, the network reflected in IC 3 appears to be involved in evaluating task-related costs and maintaining effort. This is consistent with the observation that the activity of IC 3 was largest for fast responses on incompatible stimuli, the most demanding condition (Fig. S4). A reduction of task-related activity in these areas may reflect a decrease in mental effort invested for solving the task.

IC 4 represented a larger solitary region of event-related deactivation in the inferior portion of the precuneus, adjacent PCC, and retrosplenial cortex, extending into the cuneus (Fig. 1*j*). This component expressed a biphasic initially negative HRF with a peak at 7 sec and a subsequent overshoot at 15 sec (Fig. 1*k*). The shape of the HRF found for IC 4 closely resembles the signal time course reported for the DMN by Weissman *et al.* (11). The location and negative hemodynamic responses identify this region as part of the DMN (16). This component also showed a differential modulation of activity by trial categories ($F_{5,60}$ 4.21, $P = 0.002$), and the largest deactivations were seen to be incompatible correct trials, which was slightly more consistent for fast ($t_{12}$ −11.03; $P < 0.001$) than slow ($t_{12}$ −9.21; $P < 0.001$) response times. This finding fits well with the observation that the hemodynamic signal is decreased in the DMN during cognitively demanding tasks (25), which has been linked to decreased metabolic activity (46). A linear trend of reduced deactivation of IC 4 preceded errors from trial $T_{-6}$ through $T_{-1}$ ($t_{12} = 2.42$, $P = 0.03$) and reached a significant difference from zero mean at the trial preceding the error $T_{-1}$ ($t_{12} = 2.39$, $P = 0.03$). This result implies that task-irrelevant default mode brain activity gradually reduces deactivation before errors occur (Fig. 1*l*). Our analysis extracted another component in the frontal medial wall with areas that belong to the DMN (IC 8, Fig. S5). This IC yielded a negative event-related HRF as well but, unlike IC4, was not characterized by a differential modulation of activity related to conflict, response time, feedback, and errors, such that we did not consider it further.

The Montreal Neurological Institute (MNI) coordinates of activation foci for all four ICs are summarized in Table S1, and the overall pattern of activations to different trial categories is shown in Fig. S4.

Correlation analysis revealed that the ICs showed a number of interrelations among each other, in particular between IC 1 and 2 ($z = 0.29 \pm 0.04$, $t = 7.88$, $P < 0.001$) and between IC 3 and 4 ($z = 0.20 \pm 0.04$, $t = 4.69$, $P < 0.001$), with weaker correlation coefficients between other pairs (Table S2).

The error frequency in upcoming trials following a sequence ($T_{-6,-1}$) in which the average preerror trends were present (Fig. 1 *c*, *f*, *i*, and *l*), i.e., increased activity in IC 1 and 4 and decreased activity in IC 2 and 3 was associated with a significant relative increase in error rate by 47.9% (Table S3).

## Discussion

The present results demonstrate that variability of performance accuracy is partly determined by the activity levels of event-related regional fMRI responses at least 6 sec before an erroneous response. Two of the four identified ICs revealed linear trends evolved >30 sec before the actual error occurred. This suggests that a relevant proportion of errors stems from both a decrease in task-related brain activity related to engagement in the task and a simultaneous relative increase in DMN activity. In other words, the concurrent gradual change in activity of IC 3 and 4 suggests that participants shift their brain activity from effortful motivated involvement in the task toward a mental state more similar to resting conditions. On trials immediately preceding errors, even sensorimotor activity was reduced, which probably reflects a lowered motor threshold. It is tempting to conclude that increasing disengagement from task-related brain activity causes errors. Indeed, the coherent linear trends in IC 3 and 4 suggest that maladaptive changes in brain states eventually leading to task errors may start much earlier than previously thought. However, committing and detecting the error seems to lead to reengagement in the task by reducing task-irrelevant brain activity (IC 4) and enhancing activity in the areas associated with effort in cognitive tasks (IC 3), which is compatible with previous research (4).

A similar reengagement in the task can be observed after feedback presented on trials with prolonged reaction times (Fig. S6). The monitoring system reflected in IC 1 showed an increase in activity in these trials, which is consistent with previous studies implicating the pMFC in monitoring of errors, conflict, and feedback (4, 13, 33). Subsequent to timing feedback, activity of the DMN (IC 4) decreased significantly. A concomitant activity increase of IC 3 was also found but failed to reach statistical significance. In sum, feedback activating the performance monitoring system seems to result in a similar "reset" of brain activity patterns as errors.

The exploration of interactions between ongoing and event-related brain activity provides important clues about the dynamics and adaptability of cognitive processes (29, 47, 48). We argue that the slow trends preceding errors in the present task stem from maladaptive changes of ongoing activity in response to external stimulation and task demand that modulate the amplitude of BOLD responses. However, given the length of these trends, it could be argued they were caused by task-unrelated spontaneous oscillations, particularly in the low-frequency range <0.1 Hz (1–3, 49), which have been linked to $1/f$ variability in behavioral measures. Although our data showed a $1/f$ pattern in the IC spectra (Fig. S7) and inverse correlations between the power at the frequency of low-frequency oscillations and BOLD, neither the occurrence of errors nor the modulation of response times followed a $1/f$ distribution or was correlated to the IC spectra. Moreover, a wavelet decomposition of the IC time-courses did not reveal a clear relationship of error occurrence and low-frequency oscillations, i.e., no accumulation of errors at very high or low coefficient amplitude, or corresponding phase relationships, i.e., many errors at peaks/troughs. These results and the "reset" of activity after alerting events such as errors and feedback speak in favor of the notion that the observed dynamics in brain activity patterns preceding errors reflect sequences of adaptive and maladaptive changes rather than spontaneous fluctuations.

Our findings extend EEG studies reporting a reduced medial frontal negativity time locked to correct responses on trials immediately preceding errors (7–9). A recent fMRI study using a stop-signal paradigm showed increased activity in the DMN on the trial before errors of commission (10). Moreover, the contingent negative variation (CNV) reflecting the preparatory action in a prefrontal–extrastriate network has been found to be reduced from ≈100 ms before the actual error (14). The CNV and the response-locked negativity on correct responses are assumed to be at least partly generated in the pre-SMA, which is part of IC 3. Our analyses identified this and additional brain regions and also specified the temporal evolution of brain states that may be instrumental in causing erroneous behavior.

Previous EEG and neuroimaging studies did not find evidence for error-predicting activity changes more than one trial ahead in time. Our findings, however, suggest that brain activity changes gradually, presumably in an attempt to economize task performance, toward an error-prone pattern. Whenever the performance monitoring system encounters an event indicating a performance problem, such as an overt error or a timing feedback on late responses, this gradual development is interrupted, and the activity pattern is reset to a state supporting the recruitment of cognitive control.

In conclusion, the current work demonstrates that brain activity patterns can be used to predict erroneous behavior for many seconds ahead in time, making it unlikely that errors solely result from momentary fluctuations in brain activity. Rather, a relevant proportion of action slips seems to result from maladaptive mechanisms of cognitive control. In routinely executed repetitive tasks, we can assume that the tendency to economize task performance leads to an inappropriate reduction of effort, thus causing errors. In the future, it may be of great value to monitor these brain states in real-world situations with appropriate devices that could be used outside the laboratory. This may help to avoid human errors, particularly during monotonous tasks in which gradual disengagement is difficult to avoid.

## Materials and Methods

We analyzed data from 13 healthy right-handed participants (22–29 years, eight female) who performed a speeded flanker task while fMRI data were recorded. Written informed consent was obtained from each participant before the start of the experiment according to the declaration of Helsinki. Details about the flanker task and relevant behavioral effects are provided in Figs. S1–S3.

**Image Acquisition.** Imaging was performed at 3 T on a Siemens Trio system equipped with the standard bird cage head coil. Twenty-two functional slices were obtained parallel to the anterior commissure–posterior commissure line (thickness, 4 mm; interslice gap, 1 mm) using a gradient-echo echo planar imaging (EPI) sequence with an echo time of 30 ms, a flip angle of 90°, a repetition time of 2,000 ms, and an acquisition time of 1,500 ms. The fMRI matrix acquired was 64 × 64 with a field of view of 19.2 cm, resulting in an in-plane resolution of 3 × 3 $mm^2$. A total of 1,309 volumes were acquired. Before the functional runs, anatomical modified driven equilibrium Fourier transform, and EPI-T1 slices in the plane with functional images were collected. The average intertrial interval amounted to 6 sec, and trial onsets were jittered ± 1.5 sec relative to volume acquisition to improve temporal sampling of the BOLD response.

**Preprocessing.** All images were realigned to the first image in the time series to correct for head movement and then normalized to the MNI reference space using SPM2 (www.fil.ion.ucl.ac.uk/spm). Normalized data were resliced to a cubic voxel size of 2 $mm^3$ and smoothed with a Gaussian kernel with 8 mm FWHM.

**ICA.** We used the rationale for group ICA proposed by Calhoun *et al.* (38, 50) implemented in the GIFT toolbox (http://icatb.sourceforge.net) and extended it with deconvolution and single-trial estimation. For clarity, we provide a detailed description of the group ICA model in *SI Text*, complementing the graphical illustration in Fig. 2. Group ICA requires that all subjects are analyzed at once, and principal component analysis (PCA) was used for compression to allow the datasets to be processed together (50). In the PCA step, data from each subject were reduced from the number of time points within the experiment ($n$ = 1,306) to 52 dimensions. We adjusted the number of dimensions that were estimated in this study heuristically to accommodate extraction of the maximum number of components that was computationally feasible and yield a high replicability of ICs across runs while consistently separating sources representing artifacts and known components of interest (22). In our

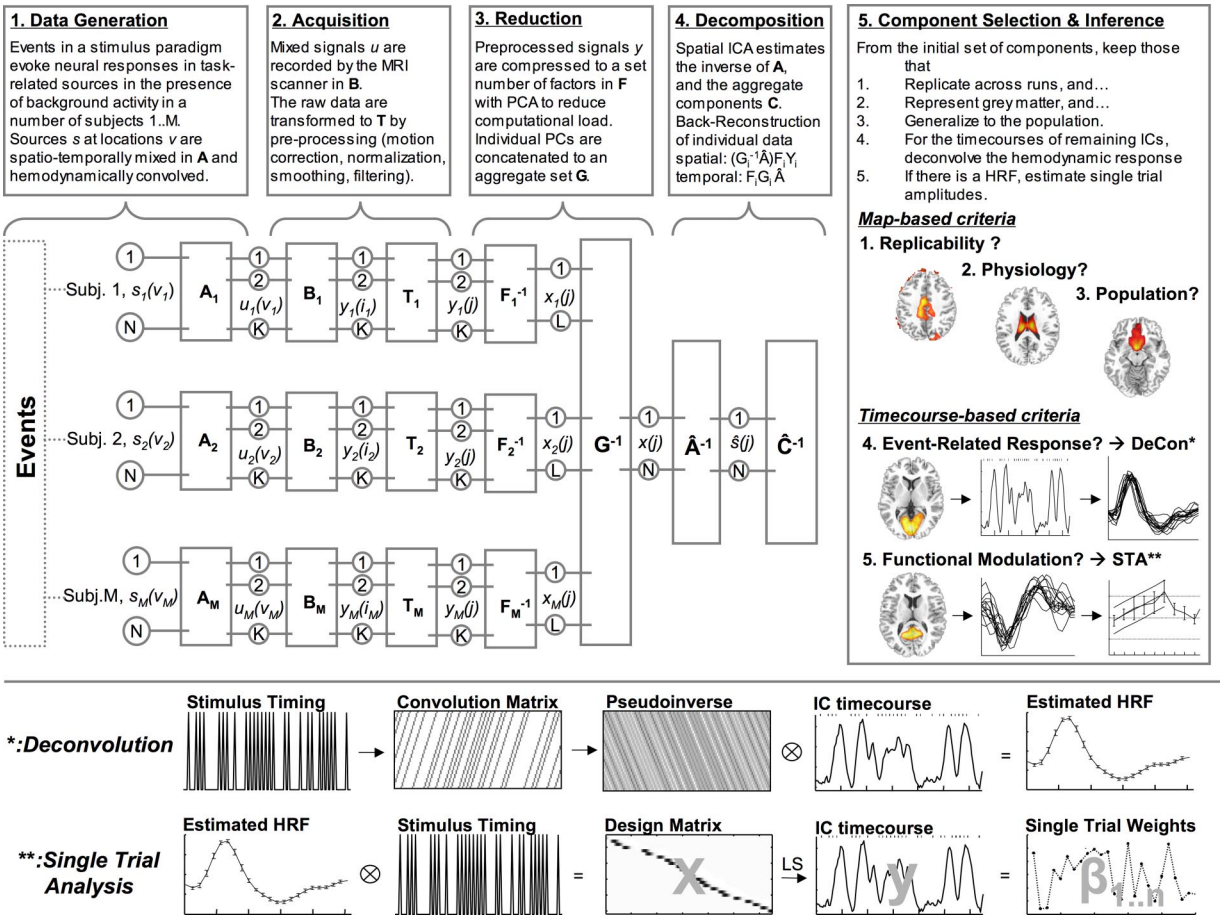


**Fig. 2.** Schematic of the group ICA analysis with deconvolution and single trial estimation. In the group ICA model, we assume that the fMRI is a linear mixture of spatially independent sources. The mixing of sources is represented by A and yields the ideal samples of brain activity $u_p(v_p)$ and the signals recorded with functional magnetic resonance imaging (*B*). Transformations (T) during preprocessing change the sampling properties. For each individual, the preprocessed data were reduced to F via PCA. Group data are generated by concatenating individual principal components in G. Spatial ICA was performed in this set, estimating aggregate components (C). Individual maps and timecourses were then back-reconstructed and inspected to identify and discard those associated with artifacts. From the remaining ICs, only those with significant maps were considered further. Then, the HRF was deconvolved by forming the convolution matrix of the stimulus onsets and multiplying the pseudoinverse with the IC timecourse. Single-trial estimation was done by fitting a design matrix (X) containing predictors for the onset times of each trial convolved with the estimated HRF onto the IC timecourse (*y*), estimating the scaling coefficients ($\beta$) of the regression model $y = \beta \cdot X + \varepsilon$. See *SI Text* for further detail.

experience, the exact choice of the number of components does not critically affect the results as long as this number is not smaller than the true dimension. Spatial ICA was then performed by using the infomax algorithm (51), with subsequent back reconstruction into single subjects. The resulting output is an independent component map and an associated IC timecourse for every component and subject, which were subjected to random effects analyses. Replicable ICs were inspected to identify and discard those primarily associated with artifacts colocalizing with gray matter (e.g., motion, flow, susceptibility; see Fig. 2 map-based criteria). From the remaining ICs, only those with significant random-effects *t* statistics of their maps, adjusted for multiple comparisons at 1% false-positive discovery rate and cluster extent of at least 27 contiguous voxels were considered further. For these ICs, the individual timecourses were filtered with a 72-sec high-pass fifth-order Butterworth digital filter, averaged across replications and normalized to unit variance.

**Deconvolution.** The event-related HRF for the ICs was then deconvolved by forming the convolution matrix of the stimulus onsets with an assumed kernel length of 20 sec and multiplying the pseudoinverse of this matrix with the IC timecourse. Single-trial estimation was performed only in ICs where consistent event-related HRFs were present, i.e., where yielding a mono-/biphasic form with a peak latency between 3 and 12 sec in all subjects. Single-trial response amplitudes were then recovered by fitting a design matrix (X) containing separate predictors for the onset times of each trial convolved with the estimated HRF onto the IC timecourse, estimating the scaling coefficients ($\beta$) in the multiple linear regression model $y = \beta \cdot X + \varepsilon$ using least squares. Single-trial $\beta$ estimates were subsequently entered into within-subjects one-sample *t* tests, and only those with significant ($P < 0.001$) differences from zero magnitude in all participants were considered further.

**Inference.** The last step in component selection was to identify the functionally relevant ICs. First, we modeled the respective single-trial weights of each subject with multiple linear regression including predictors coding for the trial type (compatible, incompatible), trial sequence (same, different), outcome (correct, error), timing feedback (''speed up,'' absent), response times, and the trial-to-trial changes of response times. Correspondingly, we tested for any significant difference between the component mean responses to the different trial categories by entering averaged weights for compatible and incompatible correct trials divided into fast and slow responses (mean split), feedback, and errors into an ANOVA with repeated measures. The subset of ICs reported here showed significant event-related responses in general; consistent effects related to response conflict, accuracy, and feedback; and differences between the conditions (Fig. S4).

Four additional ICs localizing to the visual system, the dorsal and ventral attentional system (35), and the anterior part of the DMN, respectively, showed robust event-related HRFs but did not appear significantly modulated by the current task and were thus not considered further for error precursor activity (Fig. S5).

In the selected components, we removed the variability associated with the aforementioned predictors with multiple regression and used the residual data to check for the presence of error-preceding activity. This was done by

generating averages from the residuals for sequences from six trials before to three trials after error responses, that is, from ≈30 to 40 sec preceding the event to 15–20 sec after it. The individual sequences were then entered into pointwise one-sample *t* tests under the assumption of zero magnitude. IC 3 and 4 were additionally tested for a linear trend expanding from trial position $T_{-6}$ through $T_{-1}$ preceding an error using linear regression. Individual $\beta$-estimates were entered into one-sample *t* tests, and effects were considered significant at $P < 0.05$.

Additionally, we assessed the connectivity among all four components by computing pairwise correlation coefficients between the single-trial estimates in each participant and subjected the coefficients to one-sample *t* tests after Fisher transformation. Results are reported in Table S2.

To estimate the predictive value of the four identified ICs for future behavior, we computed the change in error frequency relative to the base rate (absolute error rate 8.7%) for current trials ($T_0$) using a linear fit across the residual activities of the four ICs in the sequence of the preceding five trials ($T_{-6}$ to $T_{-1}$) for all single-trial sequences pooled across all participants. Based on a mean split of the beta weights of the linear fit in the four ICs, we generated 16 nonoverlapping classes of trials for which we computed the error frequency at $T_0$ and the proportion of feedback trials, Compatible trials and average residual response time (after removal of categorical effects from the raw response times) at $T_{-1}$ to control for these possible confounds. Results are reported in Table S3.

**ACKNOWLEDGMENTS.** We are grateful to two anonymous referees for thoughtful comments. The present study was financially supported with grants from the Research Council of Norway (to K.H.), a grant from the Deutsche Forschungsgemeinschaft Priority Program Executive Functions (to M.U.), and Grant 1 R01 EB 000840 from the National Institutes of Health (to V.D.C.).

1. Fox MD, Snyder AZ, Zacks JM, Raichle ME (2006) Coherent spontaneous activity accounts for trial-to-trial variability in human evoked brain responses. *Nat Neurosci* 9:23–25.
2. Fox MD, Raichle ME (2007) Spontaneous fluctuations in brain activity observed with functional magnetic resonance imaging. *Nat Rev Neurosci* 8:700–711.
3. Fox MD, Snyder AZ, Vincent JL, Raichle ME (2007) Intrinsic fluctuations within cortical systems account for intertrial variability in human behavior. *Neuron* 56:171–184.
4. Ridderinkhof KR, Ullsperger M, Crone EA, Nieuwenhuis S (2004) The role of the medial frontal cortex in cognitive control. *Science* 306:443–447.
5. Ullsperger M, von Cramon DY (2004) Neuroimaging of performance monitoring: error detection and beyond. *Cortex* 40:593–604.
6. Rushworth MF, *et al.* (2007) Functional organization of the medial frontal cortex. *Curr Opin Neurobiol* 17:220–227.
7. Ridderinkhof KR, Nieuwenhuis S, Bashore TR (2003) Errors are foreshadowed in brain potentials associated with action monitoring in cingulate cortex in humans. *Neurosci Lett* 348:1–4.
8. Allain S, *et al.* (2004) The modulation of the Ne-like wave on correct responses foreshadows errors. *Neurosci Lett* 372:161–166.
9. Hajcak G, Nieuwenhuis S, Ridderinkhof KR, Simons RF (2005) Error-preceding brain activity: robustness, temporal dynamics, and boundary conditions. *Biol Psychol* 70:67–78.
10. Li CS, Yan P, Bergquist KL, Sinha R (2007) Greater activation of the ''default'' brain regions predicts stop signal errors. *NeuroImage* 38:640–648.
11. Weissman DH, Roberts KC, Visscher KM, Woldorff MG (2006) The neural bases of momentary lapses in attention. *Nat Neurosci* 9:971–978.
12. Botvinick MM, Cohen JD, Carter CS (2004) Conflict monitoring and anterior cingulate cortex: an update. *Trends Cognit Sci* 8:539–546.
13. Holroyd CB, *et al.* (2004) Dorsal anterior cingulate cortex shows fMRI response to internal and external error signals. *Nat Neurosci* 7:497–498.
14. Padilla ML, Wood RA, Hale LA, Knight RT (2006) Lapses in a prefrontal-extrastriate preparatory attention network predict mistakes. *J Cognit Neurosci* 18:1477–1487.
15. Gusnard DA, Raichle ME (2001) Searching for a baseline: functional imaging and the resting human brain. *Nat Rev Neurosci* 2:685–694.
16. Raichle ME, *et al.* (2001) A default mode of brain function. *Proc Natl Acad Sci USA* 98:676–682.
17. Greicius MD, Krasnow B, Reiss AL, Menon V (2003) Functional connectivity in the resting brain: a network analysis of the default mode hypothesis. *Proc Natl Acad Sci USA* 100:253–258.
18. Horovitz SG, *et al.* (2008) Low frequency BOLD fluctuations during resting wakefulness and light sleep: A simultaneous EEG-fMRI study. *Hum Brain Mapp*, in press.
19. Greicius MD., *et al.* (2008) Persistent default-mode network connectivity during light sedation. *Hum Brain Mapp*, in press.
20. Fair DA, *et al.* (2007) A method for using blocked and event-related fMRI data to study ''resting state'' functional connectivity. *NeuroImage* 35:396–405.
21. Fox MD, *et al.* (2005) The human brain is intrinsically organized into dynamic, anticorrelated functional networks. *Proc Natl Acad Sci USA* 102:9673–9678.
22. Damoiseaux JS, *et al.* (2006) Consistent resting-state networks across healthy subjects. *Proc Natl Acad Sci USA* 103:13848–13853.
23. Greicius MD, Menon V (2004) Default-mode activity during a passive sensory task: uncoupled from deactivation but impacting activation. *J Cognit Neurosci* 16:1484–1492.
24. Malinen S, Hlushchuk Y, Hari R (2007) Towards natural stimulation in fMRI–issues of data analysis. *NeuroImage* 35:131–139.
25. Esposito F, *et al.* (2006) Independent component model of the default-mode brain function: Assessing the impact of active thinking. *Brain Res Bull* 70:263–269.
26. Mantini D, *et al.* (2007) Electrophysiological signatures of resting state networks in the human brain. *Proc Natl Acad Sci USA* 104:13170–13175.
27. Laufs H, *et al.* (2003) Electroencephalographic signatures of attentional and cognitive default modes in spontaneous brain activity fluctuations at rest. *Proc Natl Acad Sci USA* 100:11053–11058.
28. Eichele T, *et al.* (2005) Assessing the spatiotemporal evolution of neuronal activation with single-trial event-related potentials and functional MRI. *Proc Natl Acad Sci USA* 102:17798–17803.
29. Raichle ME (2006) Neuroscience. The brain's dark energy. *Science* 314:1249–1250.
30. Raichle ME, Snyder AZ (2007) A default mode of brain function: a brief history of an evolving idea. *NeuroImage* 37:1083–1090; discussion 1097–1099.
31. Morcom AM, Fletcher PC (2007) Does the brain have a baseline? Why we should be resisting a rest. *NeuroImage* 37:1073–1082.
32. Gratton G, *et al.* (1988) Pre- and poststimulus activation of response channels: a psychophysiological analysis. *J Exp Psychol* 14:331–344.
33. Ullsperger M, von Cramon DY (2001) Subprocesses of performance monitoring: a dissociation of error processing and response competition revealed by event-related fMRI and ERPs. *NeuroImage* 14:1387–1401.
34. Ullsperger M, Nittono H, von Cramon DY (2007) When goals are missed: Dealing with self-generated and externally induced failure. *NeuroImage* 35:1356–1364.
35. Corbetta M, Shulman GL (2002) Control of goal-directed and stimulus-driven attention in the brain. *Nat Rev Neurosci* 3:201–215.
36. Debener S, *et al.* (2005) Trial-by-trial coupling of concurrent electroencephalogram and functional magnetic resonance imaging identifies the dynamics of performance monitoring. *J Neurosci* 25:11730–11737.
37. Stone JV (2002) Independent component analysis: an introduction. *Trends Cognit Sci* 6:59–64.
38. Calhoun V, Adali T (2006) Unmixing fMRI with independent component analysis. *IEEE Eng Med Biol Mag* 25:79–90.
39. Aguirre GK, Zarahn E, D'Esposito M (1998) The variability of human, BOLD hemodynamic responses. *NeuroImage* 8:360–369.
40. Handwerker DA, Ollinger JM, D'Esposito M (2004) Variation of BOLD hemodynamic responses across subjects and brain regions and their effects on statistical analyses. *NeuroImage* 21:1639–1651.
41. Scholz VH, *et al.* (2000) Laterality, somatotopy and reproducibility of the basal ganglia and motor cortex during motor tasks. *Brain Res* 879:204–215.
42. Taylor SF, *et al.* (2004) A functional neuroimaging study of motivation and executive function. *NeuroImage* 21:1045–1054.
43. Dosenbach NU, *et al.* (2007) Distinct brain networks for adaptive and stable task control in humans. *Proc Natl Acad Sci USA* 104:11073–11078.
44. Schweimer J, Saft S, Hauber W (2005) Involvement of catecholamine neurotransmission in the rat anterior cingulate in effort-related decision making. *Behav Neurosci* 119:1687–1692.
45. Rudebeck PH, *et al.* (2006) Separate neural pathways process different decision costs. *Nat Neurosci* 9:1161–1168.
46. Raichle ME, Mintun MA (2006) Brain work and brain imaging. *Annu Rev Neurosci* 29:449–476.
47. Arieli A, Sterkin A, Grinvald A, Aertsen A (1996) Dynamics of ongoing activity: explanation of the large variability in evoked cortical responses. *Science* 273:1868–1871.
48. Debener S, Ullsperger M, Siegel M, Engel AK (2006) Single-trial EEG-fMRI reveals the dynamics of cognitive function. *Trends Cognit Sci* 10:558–563.
49. Leopold DA, Murayama Y, Logothetis NK (2003) Very slow activity fluctuations in monkey visual cortex: implications for functional brain imaging. *Cereb Cortex* 13:422–433.
50. Calhoun VD, Adali T, Pearlson GD, Pekar JJ (2001) A method for making group inferences from functional MRI data using independent component analysis. *Hum Brain Mapp* 14:140–151.
51. Bell AJ, Sejnowski TJ (1995) An information-maximization approach to blind separation and blind deconvolution. *Neural Comput* 7:1129–1159.